BBA - Biomembranes 1862 (2020) 183404

Contents lists available at ScienceDirect

BBA - Biomembranes

journal homepage: www.elsevier.com/locate/bbamem

^{2}H nuclear magnetic resonance spectroscopy supports larger amplitude fast motion and interference with lipid chain ordering for membrane that contains β sheet human immunodeficiency virus gp41 fusion peptide or helical hairpin influenza virus hemagglutinin fusion peptide at fusogenic pH

Ujjayini Ghosh, David P. Weliky*

Department of Chemistry, Michigan State University, East Lansing, MI 48824, USA

ARTICLE INFO

Keywords:
HIV
Influenza
NMR
Hemagglutinin
gp41
Fusion peptide

ABSTRACT

Enveloped viruses are surrounded by a membrane which is obtained from an infected host cell during budding. Infection of a new cell requires joining (fusion) of the virus and cell membranes. This process is mediated by a monotopic viral fusion protein with a large ectodomain outside the virus. The ectodomains of class I enveloped viruses have a N-terminal "fusion peptide" (fp) domain that is critical for fusion and binds to the cell membrane. In this study, ^{2}H NMR spectra are analyzed for deuterated membrane with fp from either HIV gp41 (GP) or influenza hemagglutinin (HA) fusion proteins. In addition, the HAfp samples are studied at more fusogenic pH 5 and less fusogenic pH 7. GPfp adopts intermolecular antiparallel β sheet structure whereas HAfp is a monomeric helical hairpin. The data are obtained for a set of temperatures between 35 and 0 °C using DMPC-d54 lipid with perdeuterated acyl chains. The DMPC has liquid-crystalline (L_α) phase with disordered chains at higher temperature and rippled gel ($P_{\beta'}$) or gel phase ($L_{\beta'}$) with ordered chains at lower temperature. At given temperature T, the no peptide and HAfp, pH 7 samples exhibit similar spectral lineshapes. Spectral broadening with reduced temperature correlates with the transition from L_α to $P_{\beta'}$ and then $L_{\beta'}$ phases. At given T, the lineshapes are narrower for HAfp, pH 5 vs. no peptide and HAfp, pH 7 samples, and even narrower for the GPfp sample. These data support larger-amplitude fast ($> 10^5$ Hz) lipid acyl chain motion for samples with fusogenic peptides, and peptide interference with chain ordering. The NMR data of the present paper correlate with insertion of these peptides into the hydrocarbon core of the membrane and support a significant fusion contribution from the resultant lipid acyl chain disorder, perhaps because of reduced barriers between the different membrane topologies in the fusion pathway. Membrane insertion and lipid perturbation appear common to both β sheet and helical hairpin peptides.

1. Introduction

Many viruses that cause human disease are enveloped by a membrane obtained during viral budding from the plasma membrane of an infected host cell. The subsequent steps of the viral life cycle include virus binding to a cell that can support replication, and then viral entry into the cell. These steps are mediated by protein complexes in the virus membrane [1–4]. The sequences are generally non-homologous for the proteins of different enveloped viruses. Human immunodeficiency virus (HIV) and influenza virus are class I enveloped viruses and their protein complexes for initial infection of a cell are respectively glycoprotein (GP) 160 and hemagglutinin (HA). The envelope protein complex is composed of three copies of a subunit that is a monotopic virus membrane protein (gp41 or HA2) with large ectodomain (ED) outside the virus, and three copies of a subunit (gp120 or HA1) that is bound to the trimer of gp41 or HA2 ED's [1,5]. The gp120 or HA1 subunits bind to specific receptors on their respective target cells, CD4 and CXCR4/CCR5 for gp120, and sialic acid for HA1. The sialic acid binding to HA1

Abbreviations: DMPC-d54, dimyristoylphosphatidylcholine with perdeuterated myristic chains; DOPC, dioleoylphosphatidylcholine; ED, ectodomain; EPR, electron paramagnetic resonance; fp, fusion peptide; GP, HIV glycoprotein; HA, hemagglutinin; HIV, human immunodeficiency virus; LUV, large unilamellar vesicle; MAS, magic-angle-spinning; NMR, nuclear magnetic resonance; POPC, 1-palmitoyl-2-oleoylphosphatidylcholine; REDOR, rotational-echo double-resonance; S_{CD}, order parameter; SE, soluble ectodomain; TM, transmembrane domain

* Corresponding author.
E-mail address: weliky@chemistry.msu.edu (D.P. Weliky).

https://doi.org/10.1016/j.bbamem.2020.183404
Received 13 February 2020; Received in revised form 27 April 2020; Accepted 19 June 2020
Available online 23 June 2020

triggers the cellular response of endocytosis of the virus, followed by endosome maturation including pH reduction to < 6. The low pH destabilizes HA2 ED/HA1 interactions which results in separation of HA1 from HA2 ED, followed by a large structural rearrangement of the HA2 ED to a final state [6]. The gp120 binding to CD4 and CXCR4/CCR5 is the trigger for gp120 separation from gp41 ED, with subsequent structural rearrangement of gp41 ED to a final state. There are high-resolution structures of much of the initial complex that contains the three gp41 ED's + three gp120's and the initial complex that contains three HA2 ED's + three HA1 [7–12]. For gp41 and HA2, there are also structures of the soluble region of the ED (SE) for the final state without gp120 or HA1, respectively [13–16].

Joining (fusion) of the virus and target cell membranes is concurrent with the viral protein separations and ED rearrangements, and results in deposition of the virus capsid and genetic material in the target cell cytoplasm. The influenza virus fuses with the membrane of the late endosome inside the cell, whereas HIV can fuse directly with the plasma membrane [17–20]. Fluorescence and electron microscopies and other experimental data support a temporal sequence of membrane fusion steps that include: (1) close apposition of the two membranes; (2) formation of a shared bilayer "stalk" and then "diaphragm" that separates the virus and cell contents (hemifusion); (3) formation of small pores in the hemifusion diaphragm that allow passage of small (< 1 kDa) molecules; (4) pore expansion with accompanying elimination of the diaphragm; and (5) a single contiguous membrane that encloses the cell and the virus capsid [3,18,21–23]. Several calculations suggest that the barrier to initial membrane apposition is the highest energy step during fusion, with energy of ~25 kcal/mol relative to the separated bilayers [3]. In our view, there aren't yet clear experimental data about the relative timings of the transformations of the membranes vs. those of the viral proteins.

The ~25-residue N-terminal segment of gp41 or HA2 is named the "fusion peptide" (fp), in part because some mutations in this segment significantly reduce fusion [24–27]. The GPfp and HAfp sequences are non-homologous, but the GPfp sequence is fairly-conserved among clades of HIV, and the HAfp sequence is highly-conserved among subtypes of influenza [28]. Fig. 1 shows the GPfp and HAfp sequences used in the present study. Both sequences bind model membranes [29,30]. The fusion significance of fp/membrane interaction is evidenced by the observation that after influenza virus fuses with vesicles, the fp and the transmembrane (TM) domain are the only HA segments that are deeply inserted in the fused membrane [31].

Most mechanistic models of envelope protein-catalyzed fusion posit fp binding to the target membrane during the structural transformation of the ED from the initial complex with the receptor-binding subunit to the final state without this subunit [1,4,32]. Some experimental data are consistent with this hypothesis, including the fp being part of the initial gp41 ED/gp120 or HA2 ED/HA1 complex, but not part of the final C-terminal SE structures of gp41 without gp120 or HA2 without HA1. Both the gp41 and HA2 SE structures are hairpins with proximity between regions closest to the fp and TM domains [13,16]. The hairpin SE structures in combination with the fp in the target membrane and TM in the virus membrane could reduce the energy needed for initial close apposition of the target and virus membranes [33,34]. As noted above, some calculations show that close apposition is the highest energy barrier in fusion. This apposition mechanism also correlates with efficient vesicle fusion induced by large gp41 and HA2 constructs that include the fp, final state SE, and in some cases TM domains [32,33,35–37].

There has been substantial study of the structures of GPfp and HAfp in membrane and in detergent-rich media like micelles and bicelles. The high-resolution structures are for peptide-only without the SE hairpin. In detergent media, GPfp is a single helix whereas HAfp is typically a helical hairpin with close packing of the two antiparallel helices [38–40]. In membrane, there are distributions of structures whose populations depend on parameters like mole fraction cholesterol and

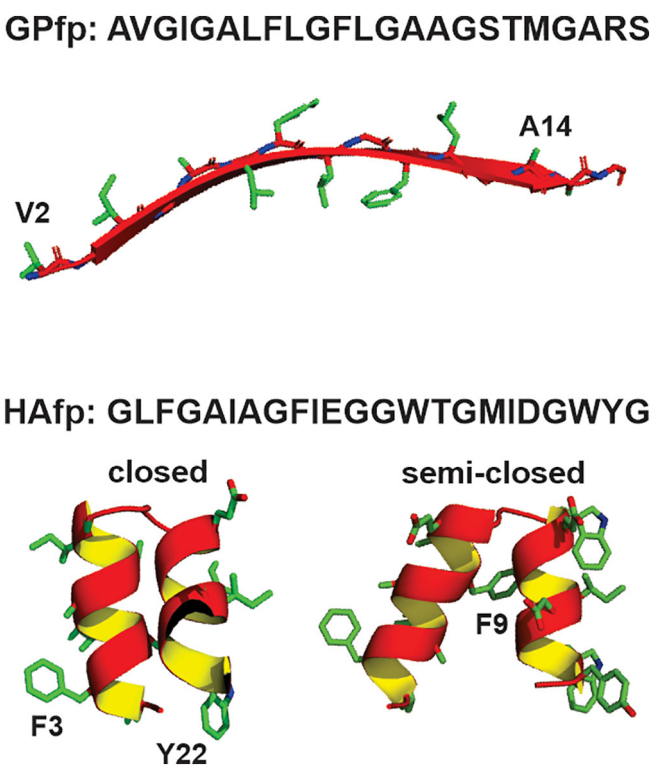

Fig. 1. Sequences and structural models of GPfp and HAfp based on data for peptide without the rest of the protein. A few residues are identified in the models. One strand of a GPfp intermolecular antiparallel β sheet is displayed. The sheets have distributions of adjacent strand registries that include the residue 1 → 16/16 → 1 and 1 → 17/17 → 1 registries. HAfp is a monomeric helical hairpin with populations of closed and semi-closed structures. The closed structure is based on PDB 2KXA.

peptide:lipid ratio [41–43]. We describe the structures that are most relevant to the present study. In membrane, GPfp is predominantly an oligomer with intermolecular antiparallel β sheet structure (Fig. 1) [44,45]. There is a distribution of adjacent strand registries that include the residue 1 → 16/16 → 1 and 1 → 17/17 → 1 registries [46]. In membrane without cholesterol, one fraction of HAfp adopts the "closed" helical hairpin structure that is also observed in detergent, while a second fraction adopts a "semi-closed" structure in which the Phe-9 ring inserts between the two helices (Fig. 1) [47–49]. There is larger semi-closed:closed population ratio at pH 5 vs. 7 that correlates with protonation of the E11 sidechain near the turn region between the two helices. HAfp-induced vesicle fusion is also higher at pH 5 vs. 7 which correlates with greater hydrophobic surface area of the semi-closed vs. closed structure. Influenza virus fusion happens at pH ≈ 5. Circular dichroism and NMR data for the fusion peptide domain in larger gp41 or HA2 constructs are generally consistent with the Fig. 1 peptide-only models [33,50–52].

As noted above, one likely fusion role of fp is binding the target membrane, which in combination with the SE structure, closely apposes the target and virus membranes. Such apposition is the first step in fusion and has ~25 kcal/mol calculated energy barrier in the absence of fusion protein. The present paper examines other possible fusion contributions from the fp that are associated with changes in the target membrane with bound fp. Earlier experimental studies have detected fp effects on membrane that include dehydration of lipid headgroups, decreased bending modulus, and increased membrane curvature [53–56]. These latter effects may facilitate formation of membrane fusion intermediate states like hemifusion that have localized regions of high curvature. In the present study, we probe another possible effect of fp's on membrane, disordering of the lipid acyl chains. Disordering

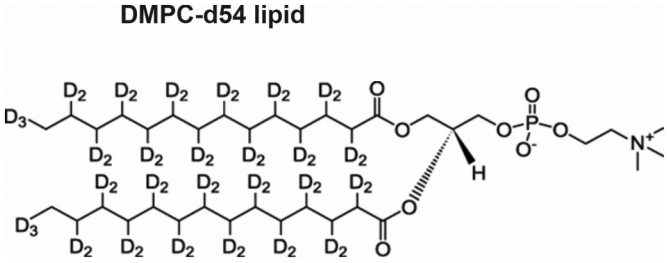

Fig. 2. Chemical structure of DMPC-d54 lipid.

seems plausible if there is fp insertion into the acyl chain region of the membrane, but analyses of experimental data from earlier studies supported differing interpretations that included ordering, no effect, or disordering, depending on the study [57–61]. Helical HAfp in membrane has also been the subject of molecular dynamics simulations, and some studies report significant acyl chain disordering, including acyl chain protrusion out of the hydrocarbon core of the membrane [60,62–64]. Such protrusion may facilitate the initial formation of an intermediate structure like the hemifusion diaphragm, with one leaflet of the diaphragm from the target membrane and one leaflet from the virus membrane.

In the present paper, ^{2}H NMR spectra are acquired and analyzed for samples prepared with dimyristoylphosphatidylcholine with perdeuterated myristoyl chains (DMPC-d54, Fig. 2) and with GPfp or HAfp at pH 5 or pH 7. The pH 5 is close to the endosome pH for influenza virus fusion and HAfp is more fusogenic at pH 5 vs. 7. ^{2}H NMR spectral lineshapes and linewidths are very useful for assessing the amplitudes of "fast" molecular motion with frequencies > 100 kHz, which is the approximate difference in quadrupolar NMR frequency between the ^{2}H-C bond parallel vs. perpendicular to the spectrometer magnetic field. For temperature > 20 °C, the DMPC acyl chains are in the liquid-crystalline (L_α) phase in which there is significant amplitude of fast motion. Peak splittings are often resolved for many of the different -C_nD sites (n = 2–14) along the myristoyl chains, and provide information about site-specific changes in motion due to bound peptide [65–68]. The variation of changes in site-specific splittings/motion also provides information about the depth of peptide insertion into the acyl chain core of the membrane. At ~20 °C, the DMPC acyl chains undergo a phase transition to the $P_{\beta'}$ rippled gel phase, and at ~10 °C, undergo a phase transition to the $L_{\beta'}$ gel phase, in which the acyl chains are ordered with all-trans conformation [69–71]. Spectra are obtained over these temperatures, and variations in their lineshapes and linewidths with bound peptide are interpreted in terms of peptide insertion and perturbation of acyl chain motion.

DMPC is a phosphatidylcholine lipid, which is typically a significant component of the target membranes of HIV and influenza, respectively the host cell plasma membrane and the late endosome membrane [72–74]. There are of course other lipids in these membranes and the lipid compositions are different between them. For the present study, GPfp and HAfp are studied in membrane with the single component DMPC. Use of the same membrane makes it more straightforward to compare the effects of GPfp vs. HAfp which have non-homologous sequences and very different structures, respectively oligomeric antiparallel β sheet and helical hairpin (Fig. 1).

2. Materials and methods

2.1. Materials

Wang resins and Fmoc protected amino acids were purchased from Peptides International (Louisville, KY), Calbiochem-Novabiochem (La Jolla, CA), and Sigma Aldrich (St. Louis, MO). DMPC-d54 lipid was purchased from Avanti Polar Lipids (Alabaster, Al). Buffers were 10 mM HEPES and 5 mM MES adjusted to either pH 5.0, 7.0, or 7.4, and contained 0.01% sodium azide as preservative.

2.2. Peptides

GPfp has sequence AVGIGALFLGFLGAAGSTMGARSWKKKKKKG and HAfp has sequence GLFGAIAGFIEGGWTGMIDGWYGGGKKKKG, and the underlined residues are respectively the N-terminal residues of the HIV gp41 and the influenza virus HA2 proteins. The GPfp sequence is from the LAV-1 laboratory strain of HIV and the HAfp sequence is from a H1 subtype of influenza virus. The C-terminal, non-underlined residues are non-native. The G and K residues increase aqueous solubility and the W in GPfp is a 280 nm absorption chromophore. GPfp and HAfp were synthesized using solid-phase peptide synthesis and Fmoc and t-Boc chemistry, respectively. A ^{13}CO label was incorporated in HAfp at Ala-5. Peptides were purified using reverse-phase HPLC with a linear gradient between two different water/acetonitrile mixtures. A C4 column was used for GPfp and a C18 column was used for HAfp. The MALDI-TOF spectrum of each purified peptide showed a prominent peak corresponding to the expected mass, and with relative intensity consistent with > 95% purity.

2.3. NMR sample preparation

Preparation of the "no peptide" sample began by weighing 44 μmol dry DMPC-d54 and then dissolving in ~2 mL of chloroform:methanol (9:1). The solvent was removed by nitrogen gas and overnight vacuum. The lipid film was suspended in ~2 mL water followed by formation of large unilamellar vesicles (LUVs) by freezing in liquid nitrogen and then thawing (> 10×). More homogeneous-diameter LUVs were prepared by repeated extrusion through a 100 nm diameter polycarbonate filter. The LUV suspension was then ultracentrifuged at 100,000g for ~4 h. The pellet was harvested, lyophilized, transferred to a 4 mm diameter NMR rotor, and then hydrated with ~20 μL of water.

The HAfp, pH 5 and HAfp, pH 7 sample preparation began with similar preparation of extruded DMPC-d54 LUVs in buffer at either pH 5.0 or pH 7.0. An aqueous solution was prepared using A_{280} with [HAfp] ≈ 150 μM, followed by dropwise addition to the LUV solution while maintaining pH. The desired HAfp:DMPC-d54 molar ratio was determined by the volume of HAfp solution that was added. The resultant proteoliposome suspension was then treated with the centrifugation, harvesting, lyophilization, transfer, and hydration protocol used for the no peptide sample. Approximately quantitative binding of HAfp to the membrane was evidenced by A_{280} < 0.01 in the supernatant after centrifugation. The final hydration in the NMR rotor was with buffer that maintained the pH of the sample. This has been the typical method previously used to prepare HAfp samples, including those for which the closed and semi-closed helical hairpin structures were detected and for which deep membrane insertion was detected [49,75].

GPfp + DMPC-d54 samples were prepared by dissolving GPfp in water with concentration determined by A_{280}, followed by pipetting an aliquot, and then lyophilization. The GPfp and 44 μmole DMPC-d54 were co-dissolved in ~2 mL 2,2,2-trifluoroethanol:chloroform:1,1,1,3,3,3-hexafluoroisopropanol (2:3:2). The solvent was removed by nitrogen gas and overnight vacuum. The lipid film was suspended in ~2 mL buffer at pH 7.4 followed by formation of LUVs by freezing in liquid nitrogen and then thawing (> 10×). The LUV suspension was then ultracentrifuged at 100,000g for ~4 h. The pellet was harvested, lyophilized, transferred to a 4 mm diameter NMR rotor, and then hydrated with ~20 μL of buffer at pH 7.4. This is a method that has previously been used to prepare GPfp samples and has resulted in predominant β sheet structure for GPfp with deep membrane insertion [75,76]. The β sheet structure and deep insertion have also been observed for GPfp samples prepared by the above "HAfp" method [75]. In addition, helical monomer structure has been detected previously for HAfp samples prepared by the "GPfp" method [42,77].

2.4. NMR spectroscopy

NMR spectra were acquired on a 9.4 T Infinity Plus spectrometer using a magic-angle-spinning (MAS) probe equipped for 4 mm diameter rotors. Nitrogen gas at defined temperature was flowed around the sample for ~1 h prior to data acquisition. ^{13}C spectra were obtained with $T_{N2} = -50$ °C, and with $^{1}H \rightarrow {}^{13}C$ cross-polarization followed by ^{13}C detection with ^{1}H decoupling. Typical NMR parameter frequencies included 8 kHz MAS, 100.8 MHz ^{13}C and 400.6 MHz ^{1}H transmitter, 50 kHz ^{1}H $\pi/2$-pulse, 50 kHz ^{1}H and 60–65 kHz ramped ^{13}C cross-polarization for 1.6 ms, 80 kHz ^{1}H decoupling, and 1 s pulse delay. Data were processed with 100 Hz Gaussian line broadening, Fourier transformation, phasing, and polynomial baseline correction. Spectra were externally-referenced to the methylene peak of adamantane at 40.5 ppm.

^{2}H NMR spectra were obtained with T_{N2} between 35 and 0 °C, which brackets the ~20 °C and ~10 °C temperatures of the respective $L_\alpha \rightarrow P_{\beta'}$ transition and $P_{\beta'} \rightarrow L_{\beta'}$ phase transitions of hydrated DMPC-d_{54}, with $L_\alpha \equiv$ liquid-crystalline, $P_{\beta'} \equiv$ rippled gel, and $L_{\beta'} \equiv$ gel phase. ^{2}H spectra were acquired without spinning and with the solid-echo pulse sequence $(\pi/2)_x - \tau - (\pi/2)_y - \tau_1$ – acquire. Typical parameters included 61.5 MHz transmitter frequency, 1.6 μs $\pi/2$ pulse (calibrated with $^{2}H_2O$), $\tau = 30$ μs, $\tau_1 = 11$ μs, dwell time = 2 μs, and recycle delay = 1 s. The phase cycle of the first $\pi/2$ pulse, second $\pi/2$ pulse, and acquisition was: $x, y, x; -x, y, -x; x, -y, x; -x, -y, -x; y, -x, y; -y, -x, -y; y, x, y; -y, x, -y$. The pulse program was written so that τ_1 included the receiver dead time, and data processing included removal of some initial acquired data so that the first datum was the peak echo. Typically 11 points were removed, so the first datum was 33 μs after the second $\pi/2$ pulse. This is comparable to $\tau = 30$ μs and is consistent with the quadrupolar spin physics. Processing also included exponential line broadening, Fourier transformation, and phasing. The spectra were externally referenced to $^{2}H_2O$ at $\nu = 0$ Hz. De-Paking was done using a NMRPipe macro that implemented a weighted fast Fourier transformation procedure [78,79].

3. Results

3.1. HAfp helical structure

Previous studies have shown that membrane-associated HAfp and GPfp have populations with either monomeric α helical or oligomeric β sheet structures in membrane [45–47,49,80]. The relative populations are assessed by comparison of relative intensities of resolved ^{13}C NMR peaks of the α helical and β sheet populations. The monomer α:oligomer β ratio is negatively-correlated with peptide:lipid molar ratio, and the ratio also depends on lipid composition, with some variation among replicate samples [41–43,81]. Fig. 3 shows the isotropic CO region of a ^{13}C MAS NMR spectrum of a sample prepared with HAfp:DMPC-d54 = 1:50 at pH 5. The HAfp was ^{13}CO labeled at Ala-5 and the spectrum exhibits a dominant feature with peak shift at 179.5 ppm. This shift correlates well with the RefDB database shift distribution for Ala ^{13}CO in helical structure, 179.4 ± 1.3 ppm, but not with the shift distribution in β strand structure, 176.1 ± 1.5 ppm [82]. The Ala-5 label contributes ~54% of the total ^{13}CO intensity. The broad background between 173 and 185 ppm is assigned to the natural abundance ^{13}CO signals from HAfp and DMPC-d54, which are ~17 and ~29% of the total intensity, respectively. The 174–178 ppm region makes the largest contribution to the broad signal and this chemical shift range correlates well with the shift range of the DMPC ^{13}CO nuclei that contribute ~65% of the natural abundance intensity [83]. There isn't detectable β sheet population for HAfp based on earlier observation of the β sheet Ala-5 ^{13}CO shift at 172 ppm and no clear peak at 172 ppm in Fig. 3 [47].

The GPfp samples of the present study likely have oligomeric antiparallel β sheet structure, based on previous ^{13}C NMR of GPfp/DMPC samples showed peak shifts that correlated with β sheet rather than α helical structure, e.g. 173 ppm for GPfp with Phe-8 ^{13}CO label [75,76]. These samples were prepared by the same method as the GPfp samples of the present study.

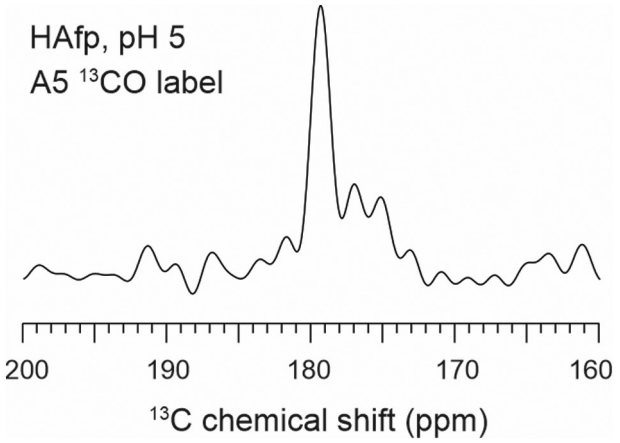

Fig. 3. Cross-polarization MAS spectrum of the isotropic ^{13}CO region of a sample with HAfp and DMPC-d54 lipid. Sample preparation was at pH 5.0 with 0.88 μmole HAfp with Ala-5 ^{13}CO label and 44 μmole DMPC-d54. The spectrum was acquired at 9.4 T with magic angle spinning at 8 kHz frequency, and the sample was cooled with nitrogen gas at −50 °C. The spectrum is the sum of 3000 scans, and was processed with 50 Hz Gaussian line broadening. The spectrum exhibits a prominent feature with peak shift at 179.5 ppm, which correlates better with the RefDB database Ala ^{13}CO shift distribution for helical structure, 179.4 ± 1.3 ppm, vs. the distribution for β strand structure, 176.1 ± 1.5 ppm.

3.2. Narrower lineshapes and higher-amplitude fast motion with fusogenic peptides

Fig. 4 displays ^{2}H NMR spectra of static samples bathed in nitrogen gas at temperatures between 35 and 0 °C. Gas was flowed around a sample for ~1 h prior to NMR data acquisition. The peptide:lipid molar ratio is 1:25. Fig. S1 displays spectra of a replicate GPfp sample which are very similar to the GPfp spectra in Fig. 4. For this temperature range, DMPC-d54 acyl chains can adopt the liquid-crystalline (L_α), rippled gel ($P_{\beta'}$), and gel phases ($L_{\beta'}$), with $L_\alpha \rightarrow P_{\beta'}$ transition at ~20 °C, and $P_{\beta'} \rightarrow L_{\beta'}$ transition at ~10 °C.

Each spectrum is the sum of individual symmetric powder patterns from the 12 -CD_2 groups and the -CD_3 group of the chains. Each group is indexed using the carbon numbering convention for myristic acid with $n = 2$ for the -CD_2 closest to the glycerol linkage and $n = 14$ for -CD_3. Each pattern will typically have a pair of symmetric "horns" which correspond to transitions of the perpendicular principal component of the ^{2}H quadrupolar tensor [65]. The width of a pattern and the horn separation is reduced by motions with frequencies much greater than the width of a static -CD group, i.e. > 100 kHz. The narrowest horn separation is for the -CD_3 group which experiences rapid rotation about the three-fold symmetry axis. The amplitude of fast motion for -CD_2 groups is typically reduced with decreasing n along the chain, and the powder patterns are correspondingly broader.

For 35, 30, and 25 °C, spectra of all samples show patterns of sharper features within the ± 20 kHz range that reflect a dominant contribution from the L_α phase [65]. The spectrum of the no peptide sample is significantly broader at 25 vs. 20 °C with fewer resolved features, which correlates with the $L_\alpha \rightarrow P_{\beta'}$ phase transition of the DMPC-d54 lipid. Relative to the L_α liquid-crystalline phase, there is smaller-amplitude fast motion in the $P_{\beta'}$ rippled gel phase. Many of the $P_{\beta'}$ lipids are packed in ordered domains with all neighboring CD_2-CD_2 groups in the extended trans conformation, and without large-amplitude axial rotation of the molecules. The no peptide spectra are even

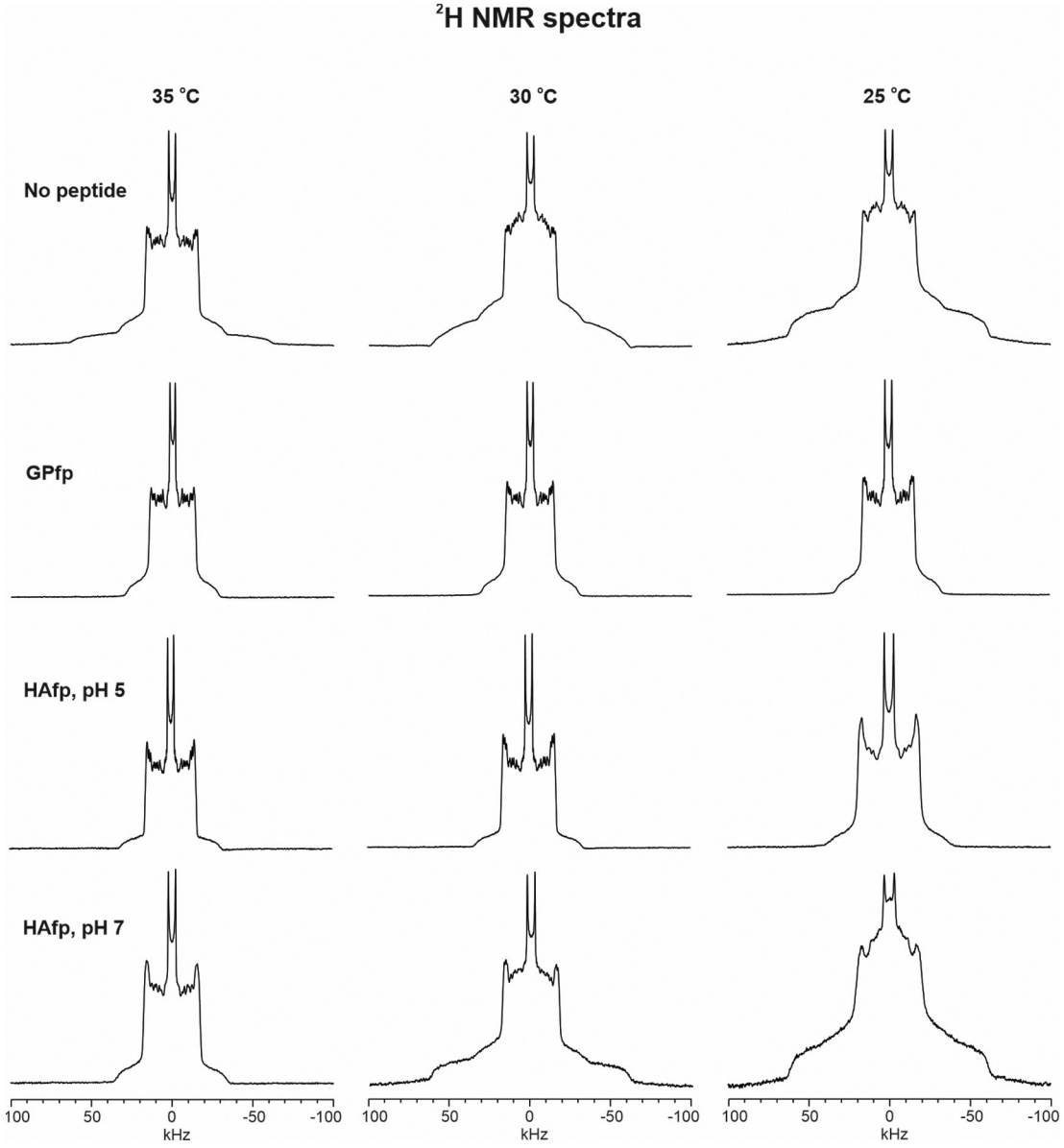

Fig. 4. Variable-temperature ^{2}H NMR spectra of static samples with DMPC-d54 and either no peptide, GPfp, HAfp, pH 5, or HAfp, pH 7. The peptide:lipid molar ratio = 1:25. Spectra were acquired with the sample bathed in nitrogen gas whose temperature was set between 35 and 0 °C, which brackets the $L_\alpha \rightarrow P_{\beta'}$ and $P_{\beta'} \rightarrow L_{\beta'}$ phase transitions of DMPC-d54. Each spectrum is typically the sum of ~5000 scans and is processed with 100 Hz exponential line broadening for 35–25 °C spectra or 500 Hz exponential line broadening for 20–0 °C spectra. Spectra are referenced to ^2H_2O with $\nu = 0$ Hz. Spectra of a replicate GPfp sample are presented in Fig. S1.

broader at 10 and 0 °C, which correlates with transition to the $P_{\beta'}$ gel phase in which all lipids are in the ordered domains.

At a given temperature of 20, 10, or 0 °C, the spectrum of the HAfp, pH 7 sample is very similar to those of the no peptide sample, which supports similar lipid phase behavior in the two samples. The spectra of the GPfp sample are different, and the 20 °C spectrum has the narrow width typical of L_α phase, and the 10 and 0 °C spectra have similar shapes and widths as the 20 °C spectra of the no peptide and HAfp, pH 7 samples. The shapes and widths of the HAfp, pH 5 sample are similar to the GPfp sample, and support reduction of the DMPC-d54 phase transition temperatures by the fusogenic peptides.

Fig. 5 displays an expanded view of spectra obtained at 35 °C, with peptide:lipid molar ratio = 1:25 and 1:50. Fig. S2 displays spectra of replicate samples which evidences reproducibility. For a particular temperature, comparison of spectra of the no peptide and 1:25 samples shows the general trend in widths GPfp < HAfp, pH 5 < no peptide < HAfp, pH 7. The effect of each peptide on spectral width is evidenced by more similar widths of the three 1:50 samples and the no peptide sample. Fig. 6 presents de-Paking analyses of the 35 °C no peptide and 1:25 spectra, i.e. the spectra expected for the membrane bilayer normal oriented parallel to the external magnetic field. Each major peak splitting ($\Delta\nu_{CD}$) of a de-Paked spectrum is assigned to specific $^2H-C_n$ of DMPC-d54. The largest $\Delta\nu_{CD}$ is considered to be a superposition of the unresolved n = 2–6 signals, and the remaining peaks are assigned using a monotonic decrease in $\Delta\nu_{CD}$ with increasing n [65–68]. There aren't clearly resolved splittings for the *sn*-1 vs. the *sn*-2 myristic chains. The order parameter for a $^2H-C_n$ segment is calculated as $S_{CD} = \Delta\nu_{CD}/334$ kHz. Table 1 lists the numerical values of S_{CD} vs. n and Fig. 7 displays plots of S_{CD}, ΔS_{CD}, and $\Delta S_{CD}/S_{CD,\text{no peptide}}$ vs. n, where $\Delta S_{CD} = S_{CD,\text{peptide}} - S_{CD,\text{no peptide}}$. The uncertainties are ± 0.002 in S_{CD}, ± 0.003 in ΔS_{CD}, and ± 0.02 in $\Delta S_{CD}/\Delta S_{\text{no peptide}}$, and are based on the variations of S_{CD} values between replicate samples, see Table S1. The S_{CD} for the no peptide sample in Table 1 are similar to earlier reported S_{CD} for DMPC-d54 without peptide, with $(S_{CD,\text{Table 1}})/$

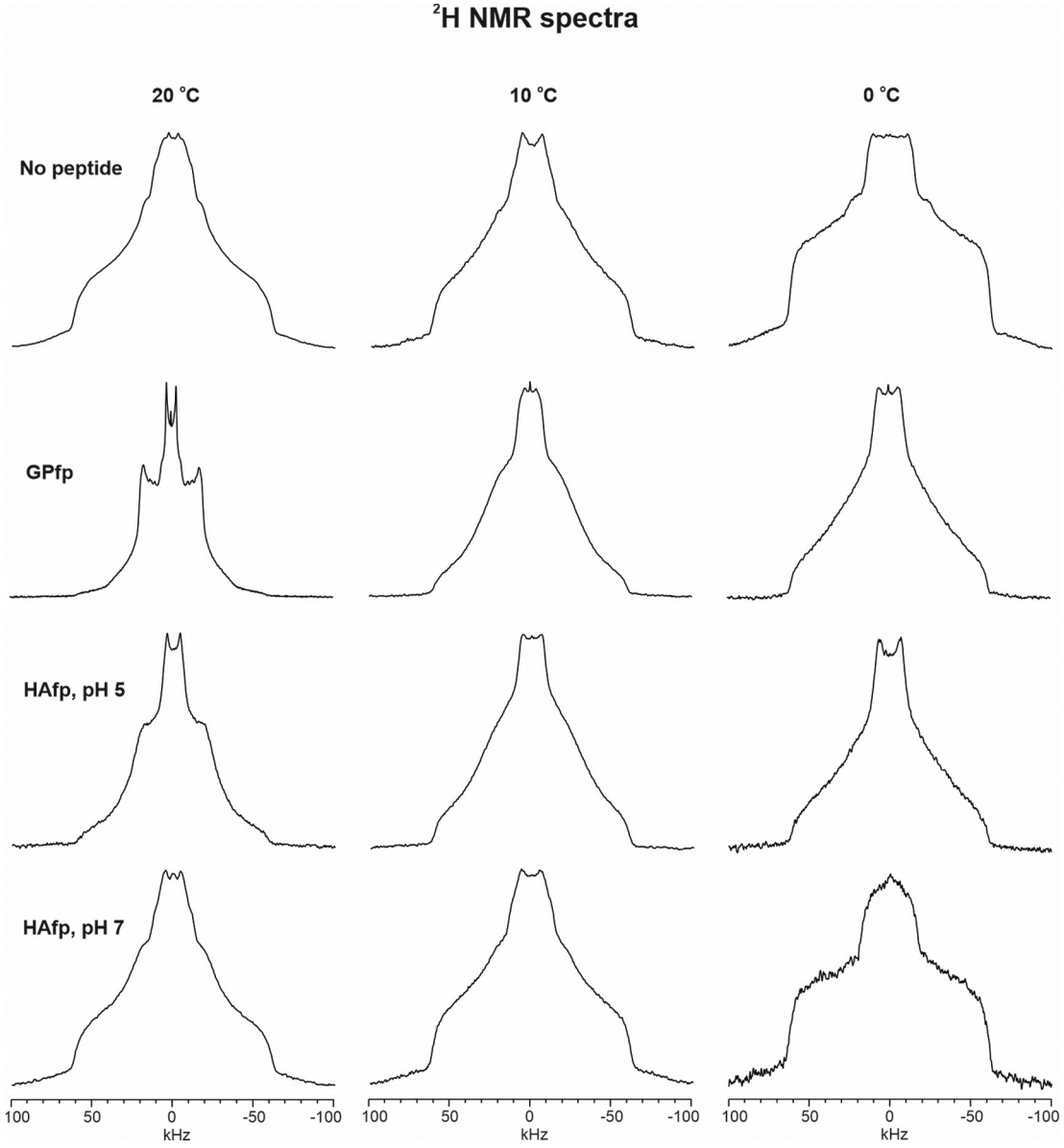

Fig. 4. (*continued*)

($S_{CD,literature}$) ≈ 1.1 [68].

4. Discussion

Fusion peptides are domains of viral fusion proteins that are critical for catalyzing joining of virus and host cell membranes. In the present paper, the effects of the fusion peptides of HIV and influenza on the perdeuterated acyl chains of DMPC-d54 lipids were probed by ^{2}H NMR spectroscopy. GPfp adopts predominant oligomeric antiparallel β sheet and HAfp adopts monomeric α helical structure. The lineshapes of the ^{2}H NMR spectra support retention of the bilayer phase with either peptide. This is consistent with some earlier studies for which the membrane has a large fraction of phosphatidycholine lipid [55,61]. Isotropic phases have sometimes been observed for membranes with fusion peptide and large fraction of phosphatidylethanolamine lipid [55,84].

Both GPfp and HAfp, pH 5 promote lipid acyl chain disorder, as evidenced by narrower spectra than the no peptide sample that reflect larger-amplitude fast motional averaging of the ^{2}H quadrupolar interaction. This narrowing is apparent at all temperatures between 35 and 0 °C, with apparent lowering by 10–20 °C of the $L_\alpha \rightarrow P_{\beta'}$ and $P_{\beta'} \rightarrow L_{\beta'}$ phase transitions that transform the disordered acyl chains into all-trans ordered conformation. By contrast, HAfp, pH 7 results in spectral lineshapes and linewidths that are similar to the no peptide sample. Fusion of the influenza virus and endosome membranes happens near pH 5 and HAfp induces more vesicle fusion at pH 5 vs. 7. There is therefore a correlation of more fusogenic peptides with lipid acyl chain disorder.

The order parameter analysis presented in Fig. 7 and Table 1 provides more site-specific analysis of the effects of the peptides on the lipid acyl chain. The $S_{CD,peptide} - S_{CD,no\ peptide} = \Delta S_{CD}$ are < 0 for fusogenic GPfp and HAfp, pH 5, and > 0 for HAfp, pH 7. The magnitude of fractional change $|\Delta S_{CD}/S_{no\ peptide}|$ has similar qualitative dependence on n for the three peptides, with larger values for the chain region nearer the tail vs. the headgroup. For n = 2–6, $\Delta S_{CD}/S_{no\ peptide} \approx -0.12$, −0.05, and 0.03 for GPfp, HAfp, pH 5, and HAfp, pH 7, respectively, and for n = 7–14, $\Delta S_{CD}/S_{no\ peptide} \approx -0.18$, −0.08, and 0.04, respectively. The intermolecular antiparallel β sheet structure of GPfp shows > 2× larger chain disordering effect vs. the monomeric HAfp α helical hairpin at pH 5.

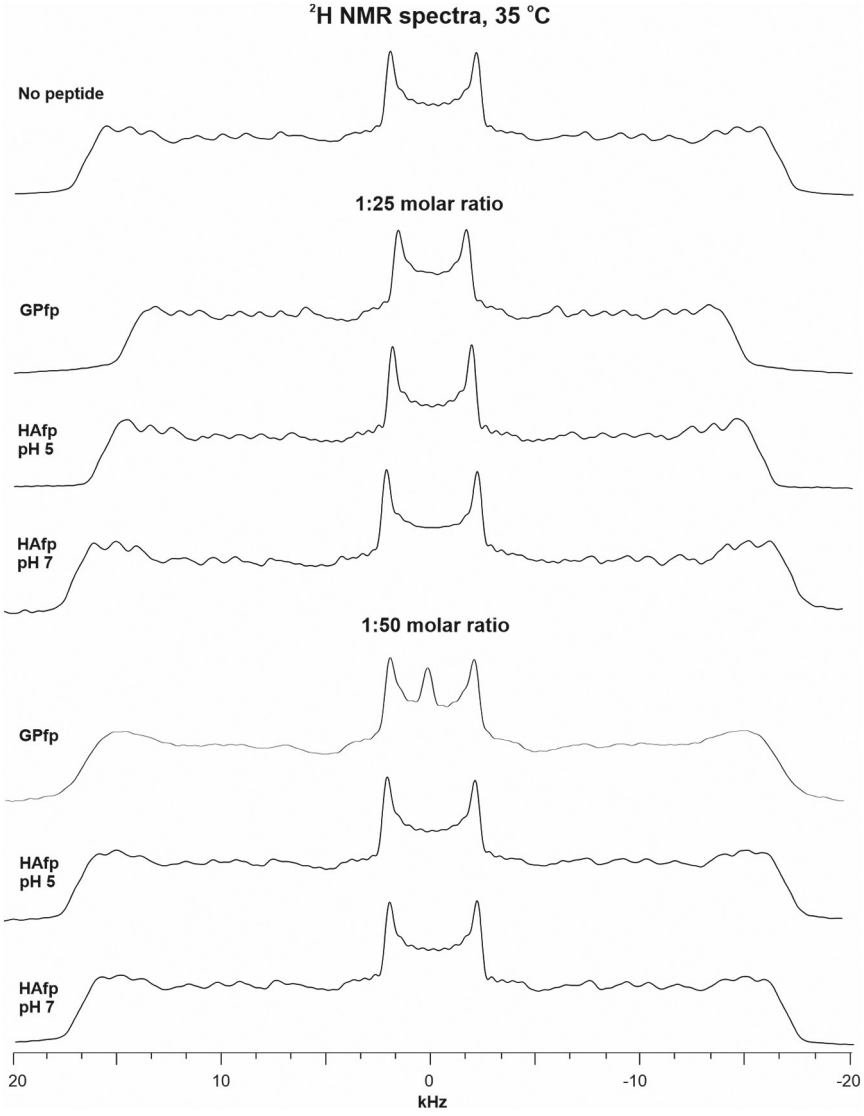

Fig. 5. ^{2}H NMR spectra at 35 °C of samples with DMPC-d54 and either no peptide, GPfp, HAfp, pH 5, or HAfp, pH 7. Spectra are displayed for peptide:lipid molar ratios = 1:25 and 1:50. Each spectrum is typically the sum of ~5000 scans and is processed with 100 Hz exponential line broadening. Spectra of replicate samples are displayed in Fig. S2.

For GPfp, the larger $|\Delta S_{CD}/S_{no\ peptide}|$ for the region closer to the tail vs. headgroup correlates with previous REDOR NMR between GPfp backbone ^{13}CO nuclei and ^{2}H nuclei in the acyl chains of phosphatidylcholine and cholesterol lipids [75,76]. There is deep membrane insertion of the GPfp β sheet, as evidenced by close (< 5 Å) contacts with ^{2}H nuclei at or near the chain termini. There is similar GPfp β sheet structure and similar GPfp REDOR results for samples prepared using organic co-solubilization like the GPfp samples of the present study and for samples prepared by aqueous binding to vesicles like the HAfp samples of the present study.

As noted above, HAfp induces acyl chain disordering at fusogenic pH 5, although less than GPfp. HAfp induces small acyl chain ordering at less fusogenic pH 7. There is also ~30% greater extent of vesicle fusion induced by HAfp at pH 5 vs. 7 [49]. Earlier NMR studies showed that HAfp adopts two related but distinct helix-turn-helix structures in membrane: "closed" with tight packing of the helical hairpin; and "semi-closed" with insertion of the Phe-9 ring between the two helices (Fig. 1). The closed and semi-closed fractions are respectively ~0.53 and 0.47 at pH 5 and ~0.68 and 0.32 at pH 7, and there is ~20% greater hydrophobic surface area for the semi-closed vs. closed structure. The samples for these earlier NMR studies were prepared in a similar manner as the HAfp samples of the present study. There are thus positive correlations between semi-closed structure and hydrophobic surface area of HAfp, lipid acyl chain disorder, and membrane fusion.

HAfp insertion into the acyl chain core correlates with larger $|\Delta S_{CD}/S_{no\ peptide}|$ for the chain region closer to the tail vs. headgroup (Fig. 7). There are other experimental data about HAfp location in membrane, but in our view there isn't yet a definitive determination. Analysis of EPR relaxation rates for site-specifically labeled HAfp were interpreted to support tilted N- and C-terminal insertion deep into a single membrane leaflet with one report of 6 Å deeper insertion at pH 5 vs. 7 [80,85]. Interpretation of these measurements is complicated by the hydrophobicity of the spin label. One molecular dynamics simulation that compared membrane location of peptide with and without spin label showed much deeper insertion with the label [86]. Both HAfp and the fp segment of full-length HA2 in detergent micelles exhibited significant hydrogen-to-deuterium exchange at pH 7.4 [34,39]. These data have been interpreted to support HAfp location at the membrane/water interface. By contrast, REDOR NMR data show that HAfp backbone ^{13}CO exhibit close (< 5 Å) contact with ^{2}H nuclei at the methyl termini of the acyl chains, and more distant contact with ^{2}H nuclei closer to the headgroups, which supports deep insertion of HAfp [75].

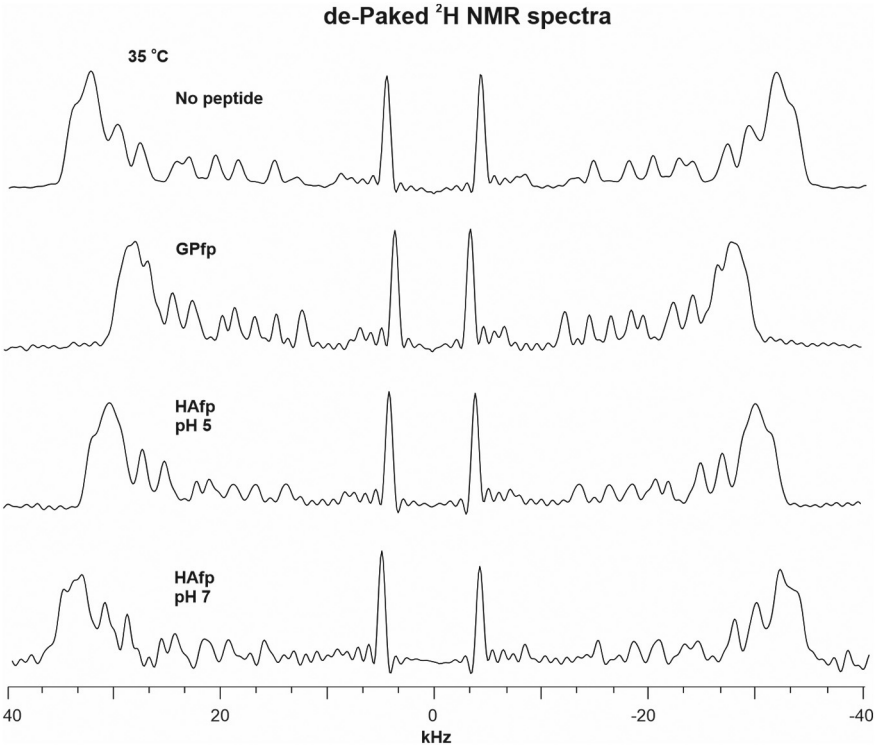

Fig. 6. De-Paking analysis of Fig. 5 no peptide and 1:25 spectra, which represent the spectra for the membrane bilayer normal parallel to the external magnetic field.

Table 1
Order parameters of DMPC-d54 at 35 °C[a,b].

Carbon number	No peptide	GPfp	HAfp	HAfp
			pH 5	pH 7
2–6	0.2538	0.2225	0.2416	0.2611
7	0.2335	0.1957	0.2163	0.2435
8	0.2181	0.1792	0.2002	0.2268
9	0.1920	0.1583	0.1781	0.2010
10	0.1829	0.1490	0.1668	0.1888
11	0.1627	0.1328	0.1500	0.1701
12	0.1445	0.1166	0.1322	0.1502
13	0.1187	0.0980	0.1106	0.1252
14	0.0350	0.0285	0.0310	0.0360

[a] Each S_{CD} order parameter is determined from a $\Delta\nu$ splitting of the de-Paked spectra of Fig. 5 with $S_{CD} = (\Delta\nu)/334$ kHz. Samples with peptide were prepared with 1:25 peptide:lipid molar ratio. Table S1 lists order parameters obtained from replicate samples.

[b] There is ± 0.002 uncertainty in S_{CD}, which is based on the variations of S_{CD} values between replicate samples, see Table S1.

The HAfp in membrane has been the subject of several molecular dynamics simulations using different methods. Membrane locations of HAfp vary between different simulations, and include the membrane/water interface, shallow insertion in a single leaflet, deep insertion in a single leaflet, and traversal of both leaflets [60,62,63,87,88]. A few of the simulations also examined effects of HAfp on the lipid molecule structure and motion including acyl chain S_{CD}. HAfp-induced acyl chain disordering is a common feature of these simulations and there is semi-quantitative agreement between the experimental $\Delta S_{CD}/S_{no\ peptide}$ of the present study (Fig. 7 and Table 1) and the simulation values. We provide a more detailed comparison of the simulation $\Delta S_{CD}/S_{no\ peptide}$ and comparison to our values for HAfp, pH 5, $\Delta S_{CD}/S_{no\ peptide} \approx -0.05$ for $n = 2$–6 and ≈ -0.08 for $n = 7$–14. For one simulation in which HAfp is located at the POPC membrane/water interface, HAfp induced palmitic chain disorder, with $\Delta S_{CD}/S_{no\ peptide} \approx -0.07$ for n = 2–4, ≈ -0.10 for $n = 5$–8, with a gradual increase to ≈ -0.03 for $n = 9$–14 [62]. For a second simulation, $\Delta S_{CD}/S_{no\ peptide} \approx -0.07$ for n = 2–6 and ~ -0.15 for n = 7–14 [60]. The first and second simulation values agree semi-quantitatively with the experimental values in Fig. 7, and in the second simulation matches the experimental observation of more negative $\Delta S_{CD}/S_{no\ peptide}$ for n = 7–14. Our experimental data provide average $\Delta S_{CD}/S_{no\ peptide}$, while the first simulation analysis also distinguishes lipids closer to vs. farther from HAfp, i.e. distance that is < 7 Å vs. > 7 Å. The farther lipids exhibit $\Delta S_{CD}/S_{no\ peptide}$ close to the average values, whereas the closer lipids exhibit much greater disorder with $\Delta S_{CD}/S_{no\ peptide} \approx -0.25$ for $n = 4$–12. However, this effect was not observed in a third simulation, and the $\Delta S_{CD}/S_{no\ peptide}$ were similar for the two lipid classes for DMPC surface-associated HAfp [63]. The second and third simulations also showed a population of HAfp that traverses the membrane. For this HAfp population, there was greater disordering for closer vs. farther lipids, with $S_{CD,closer}/S_{CD,farther} \approx ½$. The smaller $\Delta S_{CD}/S_{no\ peptide}$ from ^{2}H NMR of the present study are more consistent with the molecular dynamics $\Delta S_{CD}/S_{no\ peptide}$ for interfacial HAfp than for transmembrane HAfp. Some of the simulations also show up to 10× greater probability of acyl chain "protrusion" out of the membrane for closer vs. farther lipids. HAfp-induced "intrusion" of lipid headgroups into the membrane has also been detected in simulations [64]. These large structural deviations of the lipids may reduce activation barriers between the different membrane topological states of membrane fusion. These deviations could also modify interpretation of data from experiments like EPR relaxation rates, peptide ^{13}C-lipid ^{2}H REDOR NMR, or H/D exchange. The typical interpretations of these data assume that the locations of lipids and water close to the peptide are similar to those in membrane without peptide.

We also make comparison to analyses of other experimental data that yielded acyl chain order parameters for membrane samples with GPfp or HAfp. One such analysis with GPfp is based on wide-angle X-ray scattering of bilayers with uniaxial alignment [58]. A single S_{CD} is reported for each sample and is interpreted as the average value of $\langle 3\cos^2\beta - 1\rangle$, where β is the angle between the axis of an acyl chain segment and the bilayer normal. For a sample with DOPC lipid and 0.062 mol fraction GPfp, the X-ray $\Delta S_{CD}/S_{no\ peptide} \approx -0.4$, with

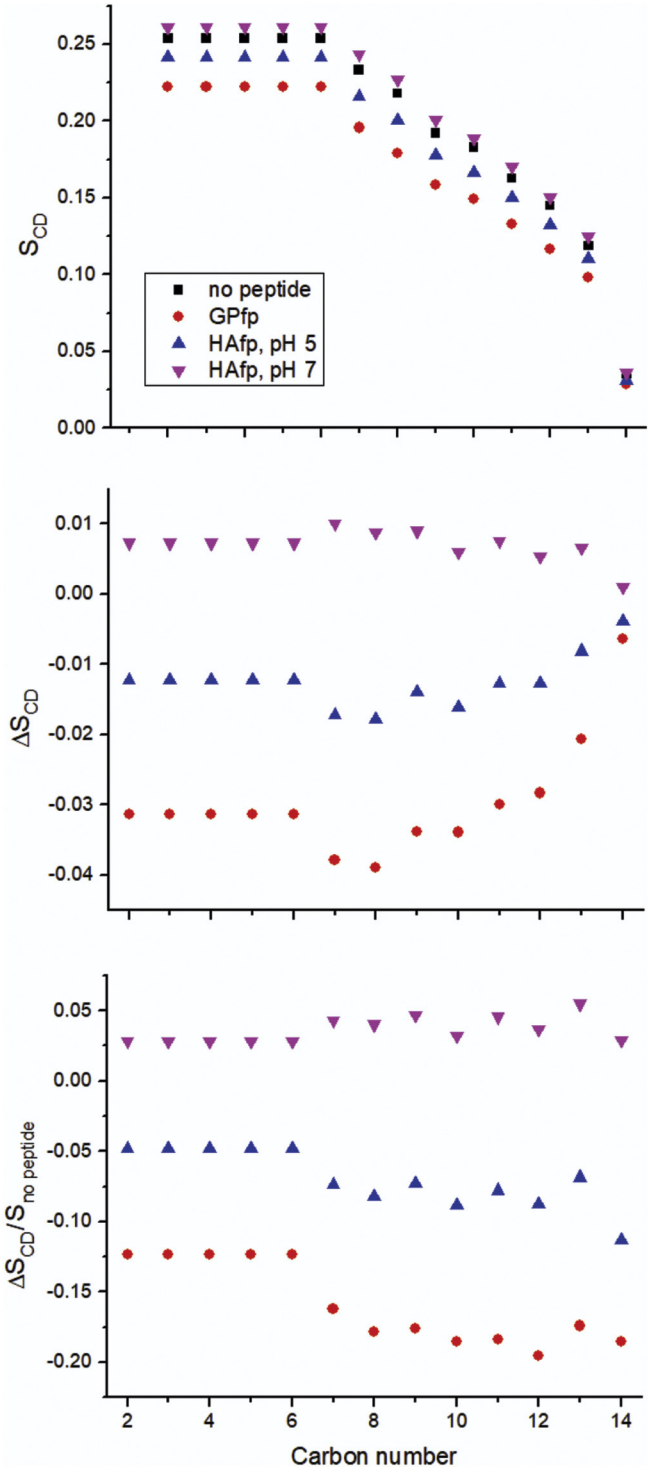

Fig. 7. Plots of (top) calculated S_{CD} order parameters, (middle) $\Delta S_{CD} = S_{CD,peptide} - S_{CD,no\ peptide}$, and (bottom) $\Delta S_{CD}/S_{CD,no\ peptide}$ vs. n (carbon numbers) of the myristic chains of DMPC-d54. The middle plot is the peptide-induced change in S_{CD} and the bottom plot is the fractional change in S_{CD}. The $S_{CD} = (\Delta\nu)/334$ kHz where $\Delta\nu$ is a quadrupolar splitting of a Fig. 6 de-Paked spectrum. The S_{CD} are the same for $n = 2$–6 because the splittings are unresolved. The S_{CD} are also presented in Table 1. The uncertainties are ± 0.002 in S_{CD}, ± 0.003 in ΔS_{CD}, and ± 0.02 in $\Delta S_{CD}/\Delta S_{no\ peptide}$, and are based on the variations of S_{CD} values between replicate samples, see Table S1.

similar values for GPfp in other lipid compositions. Both the earlier X-ray and the present and earlier NMR studies support disordering of acyl chains by GPfp [61]. There is ~1.5× greater mole fraction GPfp and ~2× greater $\Delta S_{CD}/S_{no\ peptide}$ for the X-ray vs. the present study. For lipid samples without peptide, the X-ray S_{CD} values are larger than any of the site-specific S_{CD} from de-Paking analysis of NMR spectra. This difference may reflect the longer timescale of fast motion in NMR vs. X-ray measurements.

Order parameters have also been determined from analysis of EPR spectra of spin labels attached to specific segments of lipids that are in phosphatidylcholine-rich membranes with bound GPfp or HAfp [57,59]. The overall result was that GPfp and HAfp induce ordering of lipids, which is opposite the disordering that was observed by ^{2}H NMR in the present study, and earlier studies using X-ray scattering and molecular dynamics simulation approaches. For the EPR studies, the peptide:lipid molar ratio was ≤1:100 and there was typically a step-wise onset of ordering around peptide:lipid ≈ 1:700. Typically, the $\Delta S_{CD}/S_{no\ peptide} \approx +0.15$, with larger $\Delta S_{CD}/S_{no\ peptide}$ for spin labels attached to the headgroup or C5 of the stearoyl chain vs. C14 of the stearoyl chain. There were larger $\Delta S_{CD}/S_{no\ peptide}$ for HAfp, pH 5 vs. 7. The NMR, X-ray, and simulation approaches detect all the lipids, whereas EPR only directly detects the spin-labeled lipid which is just 0.5 mol% of the total lipid. The spin label is a NO radical in a rigid 5-membered ring **C**($(CH_2)_2$)-**N**(O)-**C**($(CH_3)_2$)-**C**(H_2)-**O** where the bold atoms form the ring and substitute the methylene hydrogens in bold -**CH_2**($(CH_2)_2$) in one of acyl chains. The label is much larger than the substituted hydrogens and may disrupt acyl chain packing. It may be that the peptide-induced ordering is specific to the acyl chains of the spin-labeled lipid rather than the majority unlabeled lipid, perhaps because of some preference of the peptide for contact with the spin label. The lipid in the NMR, X-ray, and simulation samples doesn't have a chemical perturbation and these approaches also probe all of the lipids in the sample. It is unlikely that the observations of disordering for NMR, X-ray, and simulation vs. ordering for EPR are due to peptide:-lipid ratio, because the NMR and X-ray experiments are done at higher ratio than EPR and the simulations are done at lower ratio. The difference is also unlikely a consequence of the timescale for averaging, as the X-ray and simulations are for shorter times, and the NMR is for longer times.

We also compare our order parameters to those obtained from ^{2}H NMR spectra of DMPC-d54 with LL-37, an antimicrobial peptide that is a single amphipathic helix at the membrane surface [66]. The LL-37 sample was prepared using an approach similar to the approach for the GPfp sample. At 35 °C, LL-37 induces acyl chain ordering, with $\Delta S_{CD}/S_{no\ peptide} \approx +0.1$ which is similar to less fusogenic HAfp, pH 7 with $\Delta S_{CD}/S_{no\ peptide} \approx +0.04$. HAfp, pH 7 may therefore be surface-associated like LL-37, with ordering of contacting lipid headgroups. By contrast, the more fusogenic GPfp and HAfp, pH 5 induce acyl chain disordering, which may be a consequence of their insertion into the acyl region. There are earlier REDOR NMR data that support a positive correlation between depth of membrane insertion and fusogenicity for GPfp constructs [89].

The samples of the present study contain DMPC lipid and the conclusion of fusion peptide-induced lipid disordering is based on the smaller S_{CD} values in the liquid-crystalline phase and on the reduced T_m of the disordered-to-ordered acyl chain phase transitions. To our knowledge, there hasn't been calorimetric study of these phase transitions for membrane with fusion peptide. There has been calorimetry for DMPC with the antimicrobial peptides LL-37 or gramicidin S, which respectively have amphiphathic α helical and antiparallel β sheet structures [66,90,91]. For both peptides, the enthalpy change associated with the $P_{\beta'} \rightarrow L_\alpha$ transition at ~24 °C is similar to the enthalpy change of DMPC without peptide. This transition occurs over a broader temperature range for the DMPC samples with peptide vs. without peptide. This breadth has been interpreted to be a consequence of the heterogeneity of lipid proximities to peptides and we expect that there would be similar broadening for calorimetry of DMPC with fusion peptides.

Although the samples of the present study contain a single lipid

DMPC, the goal is to understand the properties of the target cell membrane with bound fusion peptide. The target membrane contains a complex mixture of lipids including cholesterol which does not have the same phases as DMPC. However, our observation of acyl chain disordering for DMPC with fusion peptide was also observed by X-ray scattering for lipid mixtures with cholesterol and fusion peptide. Disordering is probably a general effect of fusion peptides that would also be manifested in cell membranes [58]. There are substantial energy barriers between the topological states of the lipid bilayers during fusion, e.g. between two apposed bilayers and a stalk and between a stalk and the hemifusion state. The high-energy transition states associated with the barriers likely have significant acyl chain disorder, so fusion peptide-induced disordering of the target membrane may reduce these activation barriers and increase the fusion rate.

Cholesterol wasn't included in our samples because of our interest in having a single composition with either helical monomer or β sheet oligomer fusion peptide, and because β sheet oligomers are the dominant HAfp structure for membrane with cholesterol [42]. We also note that the specific lipid compositions aren't known for the target membranes of influenza and HIV. For influenza, the lipid composition of the endosome membrane changes during maturation in part because endosomes are also used for cholesterol transport [72,92]. Influenza virus fusion with vesicles is also fairly independent of the lipid compositions of the vesicles [93]. For HIV, there are microscopy and other experiments showing direct fusion with the plasma membrane as well as endocytosis followed by fusion with the endosome membrane [18]. For direct fusion, there are conflicting data about whether or not fusion occurs in specific domains, and also some data supporting fusion at domain boundaries [94–96].

5. Summary

The present study focuses on ^{2}H NMR spectra of membrane with DMPC-d54 lipid and fusion peptide from either the HIV gp41 or influenza virus HA2 proteins. The GPfp samples were prepared at pH 7.4, which is the pH of HIV/host cell fusion, and the HAfp samples were prepared at pH 5, which is close to the pH of influenza virus/late endosome fusion, and at pH 7, for which there is less fusion. GPfp is an oligomer with intermolecular antiparallel β sheet structure, and HAfp is a monomer with helical hairpin structures. Spectra were obtained at temperatures between 35 and 0 °C, which encompasses phase transitions between liquid-crystalline and gel lipid phases, with respective disordered and ordered all-trans conformations of the myristic chains. The lineshapes of the ^{2}H NMR spectra are affected by the amplitudes of motions with frequencies > 100 KHz, with larger amplitudes resulting in narrower lineshapes. At a given temperature, there are similar lineshapes and linewidths of the no peptide and HAfp, pH 7 samples, and narrower lineshapes for the GPfp and HAfp, pH 5 samples. The lineshapes and linewidths of the GPfp and HAfp, pH 5 samples at 0 °C are similar to those of the no peptide and HAfp, pH 7 samples at 20 °C. The data are consistent with disordering of acyl chains by fusogenic peptides. In addition, site-specific order parameters S_{CD} were determined from de-Paking analysis of the 35 °C spectra, followed by calculations of $\Delta S_{CD} = S_{CD,peptide} - S_{CD,no\ peptide}$, and $\Delta S_{CD}/S_{CD,no\ peptide}$. The $\Delta S_{CD}/S_{CD,no\ peptide} < 0$ for the fusogenic GPfp and HAfp, pH 5, which is consistent with chain disordering. The intermolecular antiparallel β sheet structure of GPfp shows > 2× larger chain disordering effect vs. the monomeric HAfp α helical hairpin at pH 5. The $|\Delta S_{CD}/S_{CD,no\ peptide}|$ are ~1.5× larger for ^{2}H closer to the tail vs. the headgroup, with $\Delta S_{CD}/S_{CD,no\ peptide} \approx -0.18$ for the terminal n = 7–14 of GPfp. These results are consistent with deep insertion of the fusogenic peptides into a single membrane leaflet. The small positive $\Delta S_{CD}/S_{CD,no\ peptide} \approx +0.04$ for less fusogenic HAfp, pH 7 may be due to its location at the membrane interface with minimal insertion in the membrane. Overall, our study provides strong experimental evidence for a correlation between acyl chain disordering and efficacy of fusion peptides, and supports a correlation between depth of insertion of the peptide in the acyl chain region and fusion. These correlations are observed both for GPfp which forms an intermolecular antiparallel β sheet, and for HAfp which adopts monomeric helical hairpin structures. Fusion peptide-induced disordering of the target membrane may reduce the large activation barriers between the different membrane topologies during fusion, e.g. the apposed bilayers → stalk and stalk → hemifusion steps, and thereby increase the fusion rate. The results of the present paper are generally consistent with earlier studies which include analysis of X-ray scattering that evidences overall disordering of acyl chains by GPfp, as well as semi-quantitative agreement between site-specific $\Delta S_{CD}/S_{CD,no\ peptide}$ for HAfp from the present study and site-specific $\Delta S_{CD}/S_{CD,no\ peptide}$ from earlier molecular dynamics simulations.

Declaration of competing interest

The authors declare that they have no known competing financial interests or personal relationships that could have appeared to influence the work reported in this paper.

Acknowledgements

We thank Dr. Daniel Holmes and Dr. Li Xie for assistance in the de-Paking analysis.

Funding

This work was supported by the National Institutes of Health grant number R01 AI047153.

Appendix A. Supplementary data

Supplementary data to this article can be found online at https://doi.org/10.1016/j.bbamem.2020.183404.

References

[1] J.M. White, S.E. Delos, M. Brecher, K. Schornberg, Structures and mechanisms of viral membrane fusion proteins: multiple variations on a common theme, Crit. Rev. Biochem. Mol. Biol. 43 (2008) 189–219.
[2] S.C. Harrison, Viral membrane fusion, Virology 479 (2015) 498–507.
[3] S. Boonstra, J.S. Blijleven, W.H. Roos, P.R. Onck, E. van der Giessen, A.M. van Oijen, Hemagglutinin-mediated membrane fusion: a biophysical perspective, Ann. Revs. Biophys. 47 (2018) 153–173.
[4] M. Kielian, Mechanisms of virus membrane fusion proteins, Annual Rev. Virol. 1 (2014) 171–189.
[5] R. Blumenthal, S. Durell, M. Viard, HIV entry and envelope glycoprotein-mediated fusion, J. Biol. Chem. 287 (2012) 40841–40849.
[6] R.F. Epand, R.M. Epand, Irreversible unfolding of the neutral pH form of influenza hemagglutinin demonstrates that it is not in a metastable state, Biochemistry 42 (2003) 5052–5057.
[7] I.A. Wilson, J.J. Skehel, D.C. Wiley, Structure of the haemagglutinin membrane glycoprotein of influenza virus at 3 A resolution, Nature 289 (1981) 366–373.
[8] D.C. Ekiert, A.K. Kashyap, J. Steel, A. Rubrum, G. Bhabha, R. Khayat, J.H. Lee, M.A. Dillon, R.E. O'Neil, A.M. Faynboym, M. Horowitz, L. Horowitz, A.B. Ward, P. Palese, R. Webby, R.A. Lerner, R.R. Bhatt, I.A. Wilson, Cross-neutralization of influenza A viruses mediated by a single antibody loop, Nature 489 (2012) 526–532.
[9] K.J. Cho, J.-H. Lee, K.W. Hong, S.-H. Kim, Y. Park, J.Y. Lee, S. Kang, S. Kim, J.H. Yang, E.-K. Kim, J.H. Seok, S. Unzai, S.Y. Park, X. Saelens, C.-J. Kim, J.-Y. Lee, C. Kang, H.-B. Oh, M.S. Chung, K.H. Kim, Insight into structural diversity of influenza virus haemagglutinin, J. Gen. Virol. 94 (2013) 1712–1722.
[10] X. Xiong, D. Corti, J. Liu, D. Pinna, M. Foglierini, L.J. Calder, S.R. Martin, Y.P. Lin, P.A. Walker, P.J. Collins, I. Monne, A.L. Suguitan Jr., C. Santos, N.J. Temperton, K. Subbarao, A. Lanzavecchia, S.J. Gamblin, J.J. Skehel, Structures of complexes formed by H5 influenza hemagglutinin with a potent broadly neutralizing human monoclonal antibody, Proc. Natl. Acad. Sci. U. S. A. 112 (2015) 9430–9435.
[11] M. Pancera, T.Q. Zhou, A. Druz, I.S. Georgiev, C. Soto, J. Gorman, J.H. Huang, P. Acharya, G.Y. Chuang, G. Ofek, G.B.E. Stewart-Jones, J. Stuckey, R.T. Bailer, M.G. Joyce, M.K. Louder, N. Tumba, Y.P. Yang, B.S. Zhang, M.S. Cohen, B.F. Haynes, J.R. Mascola, L. Morris, J.B. Munro, S.C. Blanchard, W. Mothes, M. Connors, P.D. Kwong, Structure and immune recognition of trimeric pre-fusion HIV-1 Env, Nature 514 (2014) 455–461.
[12] A.B. Ward, I.A. Wilson, The HIV-1 envelope glycoprotein structure: nailing down a

moving target, Immunol. Rev. 275 (2017) 21–32.
[13] J. Chen, J.J. Skehel, D.C. Wiley, N- and C-terminal residues combine in the fusion-pH influenza hemagglutinin HA_2 subunit to form an N cap that terminates the triple-stranded coiled coil, Proc. Natl. Acad. Sci. U. S. A. 96 (1999) 8967–8972.
[14] M. Caffrey, M. Cai, J. Kaufman, S.J. Stahl, P.T. Wingfield, D.G. Covell, A.M. Gronenborn, G.M. Clore, Three-dimensional solution structure of the 44 kDa ectodomain of SIV gp41, EMBO J. 17 (1998) 4572–4584.
[15] Z.N. Yang, T.C. Mueser, J. Kaufman, S.J. Stahl, P.T. Wingfield, C.C. Hyde, The crystal structure of the SIV gp41 ectodomain at 1.47 A resolution, J. Struct. Biol. 126 (1999) 131–144.
[16] V. Buzon, G. Natrajan, D. Schibli, F. Campelo, M.M. Kozlov, W. Weissenhorn, Crystal structure of HIV-1 gp41 including both fusion peptide and membrane proximal external regions, PLoS Pathog. 6 (2010) e1000880.
[17] M. Lakadamyali, M.J. Rust, H.P. Babcock, X.W. Zhuang, Visualizing infection of individual influenza viruses, Proc. Natl. Acad. Sci. U. S. A. 100 (2003) 9280–9285.
[18] C. Grewe, A. Beck, H.R. Gelderblom, HIV: early virus-cell interactions, J. AIDS 3 (1990) 965–974.
[19] G.B. Melikyan, HIV entry: a game of hide-and-fuse? Curr. Opin. Virol. 4 (2014) 1–7.
[20] N. Herold, M. Anders-Osswein, B. Glass, M. Eckhardt, B. Muller, H.G. Krausslich, HIV-1 entry in SupT1-R5, CEM-ss, and primary CD4(+) T cells occurs at the plasma membrane and does not require endocytosis, J. Virol. 88 (2014) 13956–13970.
[21] G.W. Kemble, T. Danieli, J.M. White, Lipid-anchored influenza hemagglutinin promotes hemifusion, not complete fusion, Cell 76 (1994) 383–391.
[22] L.V. Chernomordik, V.A. Frolov, E. Leikina, P. Bronk, J. Zimmerberg, The pathway of membrane fusion catalyzed by influenza hemagglutinin: restriction of lipids, hemifusion, and lipidic fusion pore formation, J. Cell Biol. 140 (1998) 1369–1382.
[23] P.I. Kuzmin, J. Zimmerberg, Y.A. Chizmadzhev, F.S. Cohen, A quantitative model for membrane fusion based on low-energy intermediates, Proc. Natl. Acad. Sci. U. S. A. 98 (2001) 7235–7240.
[24] S.R. Durell, I. Martin, J.M. Ruysschaert, Y. Shai, R. Blumenthal, What studies of fusion peptides tell us about viral envelope glycoprotein-mediated membrane fusion, Mol. Membr. Biol. 14 (1997) 97–112.
[25] E.O. Freed, E.L. Delwart, G.L. Buchschacher Jr., A.T. Panganiban, A mutation in the human immunodeficiency virus type 1 transmembrane glycoprotein gp41 dominantly interferes with fusion and infectivity, Proc. Natl. Acad. Sci. U. S. A. 89 (1992) 70–74.
[26] H. Qiao, R.T. Armstrong, G.B. Melikyan, F.S. Cohen, J.M. White, A specific point mutant at position 1 of the influenza hemagglutinin fusion peptide displays a hemifusion phenotype, Mol. Biol. Cell 10 (1999) 2759–2769.
[27] K.E. Zawada, K. Okamoto, P.M. Kasson, Influenza hemifusion phenotype depends on membrane context: differences in cell-cell and virus-cell fusion, J. Mol. Biol. 430 (2018) 594–601.
[28] E. Nobusawa, T. Aoyama, H. Kato, Y. Suzuki, Y. Tateno, K. Nakajima, Comparison of complete amino acid sequences and receptor binding properties among 13 serotypes of hemagglutinins of influenza A viruses, Virology 182 (1991) 475–485.
[29] X. Han, L.K. Tamm, A host-guest system to study structure-function relationships of membrane fusion peptides, Proc. Natl. Acad. Sci. U. S. A. 97 (2000) 13097–13102.
[30] J. Yang, M. Prorok, F.J. Castellino, D.P. Weliky, Oligomeric β-structure of the membrane-bound HIV-1 fusion peptide formed from soluble monomers, Biophys. J. 87 (2004) 1951–1963.
[31] P. Durrer, C. Galli, S. Hoenke, C. Corti, R. Gluck, T. Vorherr, J. Brunner, H+-induced membrane insertion of influenza virus hemagglutinin involves the HA2 amino-terminal fusion peptide but not the coiled coil region, J. Biol. Chem. 271 (1996) 13417–13421.
[32] K. Banerjee, D.P. Weliky, Folded monomers and hexamers of the ectodomain of the HIV gp41 membrane fusion protein: potential roles in fusion and synergy between the fusion peptide, hairpin, and membrane-proximal external region, Biochemistry 53 (2014) 7184–7198.
[33] A. Ranaweera, P.U. Ratnayake, D.P. Weliky, The stabilities of the soluble ectodomain and fusion peptide hairpins of the influenza virus hemagglutinin subunit II protein are positively correlated with membrane fusion, Biochemistry 57 (2018) 5480–5493.
[34] A. Ranaweera, P.U. Ratnayake, E.A.P. Ekanayaka, R. Declercq, D.P. Weliky, Hydrogen-deuterium exchange supports independent membrane-interfacial fusion peptide and transmembrane domains in subunit 2 of influenza virus hemagglutinin protein, a structured and aqueous-protected connection between the fusion peptide and soluble ectodomain, and the importance of membrane apposition by the trimer-of-hairpins structure, Biochemistry 58 (2019) 2432–2446.
[35] P.U. Ratnayake, E.A.P. Ekanayaka, S.S. Komanduru, D.P. Weliky, Full-length trimeric influenza virus hemagglutinin II membrane fusion protein and shorter constructs lacking the fusion peptide or transmembrane domain: hyperthermostability of the full-length protein and the soluble ectodomain and fusion peptide make significant contributions to fusion of membrane vesicles, Protein Expr. Purif. 117 (2016) 6–16.
[36] S. Liang, P.U. Ratnayake, C. Keinath, L. Jia, R. Wolfe, A. Ranaweera, D.P. Weliky, Efficient fusion at neutral pH by human immunodeficiency virus gp41 trimers containing the fusion peptide and transmembrane domains, Biochemistry 57 (2018) 1219–1235.
[37] R.F. Epand, J.C. Macosko, C.J. Russell, Y.K. Shin, R.M. Epand, The ectodomain of HA2 of influenza virus promotes rapid pH dependent membrane fusion, J. Mol. Biol. 286 (1999) 489–503.
[38] C.P. Jaroniec, J.D. Kaufman, S.J. Stahl, M. Viard, R. Blumenthal, P.T. Wingfield, A. Bax, Structure and dynamics of micelle-associated human immunodeficiency virus gp41 fusion domain, Biochemistry 44 (2005) 16167–16180.
[39] J.L. Lorieau, J.M. Louis, A. Bax, The complete influenza hemagglutinin fusion domain adopts a tight helical hairpin arrangement at the lipid:water interface, Proc. Natl. Acad. Sci. U. S. A. 107 (2010) 11341–11346.
[40] T.P. Du, L. Jiang, M.L. Liu, NMR structures of fusion peptide from influenza hemagglutinin H3 subtype and its mutants, J. Peptide Sci. 20 (2014) 292–297.
[41] J. Yang, P.D. Parkanzky, M.L. Bodner, C.G. Duskin, D.P. Weliky, Application of REDOR subtraction for filtered MAS observation of labeled backbone carbons of membrane-bound fusion peptides, J. Magn. Reson. 159 (2002) 101–110.
[42] C.M. Wasniewski, P.D. Parkanzky, M.L. Bodner, D.P. Weliky, Solid-state nuclear magnetic resonance studies of HIV and influenza fusion peptide orientations in membrane bilayers using stacked glass plate samples, Chem. Phys. Lipids 132 (2004) 89–100.
[43] W. Qiang, D.P. Weliky, HIV fusion peptide and its cross-linked oligomers: efficient syntheses, significance of the trimer in fusion activity, correlation of β strand conformation with membrane cholesterol, and proximity to lipid headgroups, Biochemistry 48 (2009) 289–301.
[44] F.B. Pereira, F.M. Goni, A. Muga, J.L. Nieva, Permeabilization and fusion of uncharged lipid vesicles induced by the HIV-1 fusion peptide adopting an extended conformation: dose and sequence effects, Biophys. J. 73 (1997) 1977–1986.
[45] W. Qiang, M.L. Bodner, D.P. Weliky, Solid-state NMR spectroscopy of human immunodeficiency virus fusion peptides associated with host-cell-like membranes: 2D correlation spectra and distance measurements support a fully extended conformation and models for specific antiparallel strand registries, J. Am. Chem. Soc. 130 (2008) 5459–5471.
[46] S.D. Schmick, D.P. Weliky, Major antiparallel and minor parallel beta sheet populations detected in the membrane-associated human immunodeficiency virus fusion peptide, Biochemistry 49 (2010) 10623–10635.
[47] Y. Sun, D.P. Weliky, ^{13}C-^{13}C correlation spectroscopy of membrane-associated influenza virus fusion peptide strongly supports a helix-turn-helix motif and two turn conformations, J. Am. Chem. Soc. 131 (2009) 13228–13229.
[48] U. Ghosh, L. Xie, D.P. Weliky, Detection of closed influenza virus hemagglutinin fusion peptide structures in membranes by backbone ^{13}CO-^{15}N rotational-echo double-resonance solid-state NMR, J. Biomol. NMR 55 (2013) 139–146.
[49] U. Ghosh, L. Xie, L.H. Jia, S. Liang, D.P. Weliky, Closed and semiclosed interhelical structures in membrane vs closed and open structures in detergent for the influenza virus hemagglutinin fusion peptide and correlation of hydrophobic surface area with fusion catalysis, J. Am. Chem. Soc. 137 (2015) 7548–7551.
[50] K. Sackett, M.J. Nethercott, Z.X. Zheng, D.P. Weliky, Solid-state NMR spectroscopy of the HIV gp41 membrane fusion protein supports intermolecular antiparallel beta sheet fusion peptide structure in the final six-helix bundle state, J. Mol. Biol. 426 (2014) 1077–1094.
[51] N.A. Lakomek, J.D. Kaufman, S.J. Stahl, J.M. Louis, A. Grishaev, P.T. Wingfield, A. Bax, Internal dynamics of the homotrimeric HIV-1 viral coat protein gp41 on multiple time scales, Angew. Chem. Int. Ed. 52 (2013) 3911–3915.
[52] P.U. Ratnayake, K. Sackett, M.J. Nethercott, D.P. Weliky, pH-dependent vesicle fusion induced by the ectodomain of the human immunodeficiency virus membrane fusion protein gp41: two kinetically distinct processes and fully-membrane-associated gp41 with predominant beta sheet fusion peptide conformation, Biochim. Biophys. Acta 1848 (2015) 289–298.
[53] R.M. Epand, R.F. Epand, I. Martin, J.M. Ruysschaert, Membrane interactions of mutated forms of the influenza fusion peptide, Biochemistry 40 (2001) 8800–8807.
[54] S. Tristram-Nagle, J.F. Nagle, HIV-1 fusion peptide decreases bending energy and promotes curved fusion intermediates, Biophys. J. 93 (2007) 2048–2055.
[55] C.M. Gabrys, R. Yang, C.M. Wasniewski, J. Yang, C.G. Canlas, W. Qiang, Y. Sun, D.P. Weliky, Nuclear magnetic resonance evidence for retention of a lamellar membrane phase with curvature in the presence of large quantities of the HIV fusion peptide, Biochim. Biophys. Acta 1798 (2010) 194–201.
[56] H.W. Yao, M. Hong, Conformation and lipid interaction of the fusion peptide of the paramyxovirus PIV5 in anionic and negative-curvature membranes from solid-state NMR, J. Am. Chem. Soc. 136 (2014) 2611–2624.
[57] M. Ge, J.H. Freed, Fusion peptide from influenza hemagglutinin increases membrane surface order: an electron-spin resonance study, Biophys. J. 96 (2009) 4925–4934.
[58] S. Tristram-Nagle, R. Chan, E. Kooijman, P. Uppamoochikkal, W. Qiang, D.P. Weliky, J.F. Nagle, HIV fusion peptide penetrates, disorders, and softens T-cell membrane mimics, J. Mol. Biol. 402 (2010) 139–153.
[59] A.L. Lai, J.H. Freed, HIV gp41 fusion peptide increases membrane ordering in a cholesterol-dependent fashion, Biophys. J. 106 (2014) 172–181.
[60] R. Worch, J. Krupa, A. Filipek, A. Szymaniec, P. Setny, Three conserved C-terminal residues of influenza fusion peptide alter its behavior at the membrane interface, Biochim. Biophys. Acta 1861 (2017) 97–105.
[61] J. Yang, P.D. Parkanzky, B.A. Khunte, C.G. Canlas, R. Yang, C.M. Gabrys, D.P. Weliky, Solid state NMR measurements of conformation and conformational distributions in the membrane-bound HIV-1 fusion peptide, J. Mol. Graph. Model. 19 (2001) 129–135.
[62] P. Larsson, P.M. Kasson, Lipid tail protrusion in simulations predicts fusogenic activity of influenza fusion peptide mutants and conformational models, PLoS Comp. Biol. 9 (2013) e1002950.
[63] B.L. Victor, D. Lousa, J.M. Antunes, C.M. Soares, Self-assembly molecular dynamics simulations shed light into the interaction of the influenza fusion peptide with a membrane bilayer, J. Chem. Inform. Model. 55 (2015) 795–805.
[64] S. Legare, P. Lagguee, The influenza fusion peptide promotes lipid polar head intrusion through hydrogen bonding with phosphates and N-terminal membrane insertion depth, Proteins-Struc. Func. Bioinform. 82 (2014) 2118–2127.
[65] M. Bloom, E. Evans, O.G. Mouritsen, Physical properties of the fluid lipid-bilayer component of cell membranes: a perspective, Q. Rev. Biophys. 24 (1991) 293–397.
[66] K.A. Henzler-Wildman, G.V. Martinez, M.F. Brown, A. Ramamoorthy, Perturbation of the hydrophobic core of lipid bilayers by the human antimicrobial peptide LL-37,

Biochemistry 43 (2004) 8459–8469.
[67] P.C. Dave, E.K. Tiburu, K. Damodaran, G.A. Lorigan, Investigating structural changes in the lipid bilayer upon insertion of the transmembrane domain of the membrane-bound protein phospholamban utilizing ^{31}P and ^{2}H solid-state NMR spectroscopy, Biophys. J. 86 (2004) 1564–1573.
[68] A. Leftin, M.F. Brown, An NMR database for simulations of membrane dynamics, Biochim. Biophys. Acta 1808 (2011) 818–839.
[69] R. Koynova, M. Caffrey, Phases and phase transitions of the phosphatidylcholines, Biochim. Biophys. Acta 1376 (1998) 91–145.
[70] D. Guardfriar, C.H. Chen, A.S. Engle, Deuterium-isotope effect on the stability of molecules - phospholipids, J. Phys. Chem. 89 (1985) 1810–1813.
[71] G.X. Wang, C.H. Chen, Thermodynamic elucidation of structural stability of deuterated biological molecules - deuterated phospholipid-vesicles in H_2O, Arch. Biochem. Biophys. 301 (1993) 330–335.
[72] T. Kobayashi, M.H. Beuchat, J. Chevallier, A. Makino, N. Mayran, J.M. Escola, C. Lebrand, P. Cosson, T. Kobayashi, J. Gruenberg, Separation and characterization of late endosomal membrane domains, J. Biol. Chem. 277 (2002) 32157–32164.
[73] S. Guha, M. Rajani, H. Padh, Identification and characterization of lipids from endosomes purified by electromagnetic chromatography, Indian J. Biochem. Biophys. 44 (2007) 443–449.
[74] M. Lorizate, T. Sachsenheimer, B. Glass, A. Habermann, M.J. Gerl, H.G. Krausslich, B. Brugger, Comparative lipidomics analysis of HIV-1 particles and their producer cell membrane in different cell lines, Cell. Microbiol. 15 (2013) 292–304.
[75] L.H. Jia, S. Liang, K. Sackett, L. Xie, U. Ghosh, D.P. Weliky, REDOR solid-state NMR as a probe of the membrane locations of membrane-associated peptides and proteins, J. Magn. Reson. 253 (2015) 154–165.
[76] L. Xie, L.H. Jia, S. Liang, D.P. Weliky, Multiple locations of peptides in the hydrocarbon core of gel-phase membranes revealed by peptide ^{13}C to lipid ^{2}H rotational-echo double-resonance solid-state nuclear magnetic resonance, Biochemistry 54 (2015) 677–684.
[77] L. Xie, U. Ghosh, S.D. Schmick, D.P. Weliky, Residue-specific membrane location of peptides and proteins using specifically and extensively deuterated lipids and ^{13}C-^{2}H rotational-echo double-resonance solid-state NMR, J. Biomol. NMR 55 (2013) 11–17.
[78] M.A. McCabe, S.R. Wassall, Rapid deconvolution of NMR powder spectra by weighted fast Fourier transformation, Solid State Nucl. Magn. Reson. 10 (1997) 53–61.
[79] M.-A. Sani, D.K. Weber, F. Delaglio, F. Separovic, J.D. Gehman, A practical implementation of de-Pake-ing via weighted Fourier transformation, PeerJ 1 (2013) e30.
[80] J.C. Macosko, C.H. Kim, Y.K. Shin, The membrane topology of the fusion peptide region of influenza hemagglutinin determined by spin-labeling EPR, J. Mol. Biol. 267 (1997) 1139–1148.
[81] M.L. Bodner, C.M. Gabrys, P.D. Parkanzky, J. Yang, C.A. Duskin, D.P. Weliky, Temperature dependence and resonance assignment of ^{13}C NMR spectra of selectively and uniformly labeled fusion peptides associated with membranes, Magn. Reson. Chem. 42 (2004) 187–194.
[82] H.Y. Zhang, S. Neal, D.S. Wishart, RefDB: a database of uniformly referenced protein chemical shifts, J. Biomol. NMR 25 (2003) 173–195.
[83] J. Yang, C.M. Gabrys, D.P. Weliky, Solid-state nuclear magnetic resonance evidence for an extended beta strand conformation of the membrane-bound HIV-1 fusion peptide, Biochemistry 40 (2001) 8126–8137.
[84] F.B. Pereira, J.M. Valpuesta, G. Basanez, F.M. Goni, J.L. Nieva, Interbilayer lipid mixing induced by the human immunodeficiency virus type-1 fusion peptide on large unilamellar vesicles: the nature of the nonlamellar intermediates, Chem. Phys. Lipids 103 (1999) 11–20.
[85] X. Han, J.H. Bushweller, D.S. Cafiso, L.K. Tamm, Membrane structure and fusion-triggering conformational change of the fusion domain from influenza hemagglutinin, Nature Struct. Biol. 8 (2001) 715–720.
[86] M. Sammalkorpi, T. Lazaridis, Modeling a spin-labeled fusion peptide in a membrane: implications for the interpretation of EPR experiments, Biophys. J. 92 (2007) 10–22.
[87] A.R. Brice, T. Lazaridis, Structure and dynamics of a fusion peptide helical hairpin on the membrane surface: comparison of molecular simulations and NMR, J. Phys. Chem. B 118 (2014) 4461–4470.
[88] J.L. Baylon, E. Tajkhorshid, Capturing spontaneous membrane insertion of the influenza virus hemagglutinin fusion peptide, J. Phys. Chem. B 119 (2015) 7882–7893.
[89] W. Qiang, Y. Sun, D.P. Weliky, A strong correlation between fusogenicity and membrane insertion depth of the HIV fusion peptide, Proc. Natl. Acad. Sci. U. S. A. 106 (2009) 15314–15319.
[90] E.J. Prenner, R. Lewis, K.C. Neuman, S.M. Gruner, L.H. Kondejewski, R.S. Hodges, R.N. McElhaney, Nonlamellar phases induced by the interaction of gramicidin S with lipid bilayers. A possible relationship to membrane-disrupting activity, Biochemistry 36 (1997) 7906–7916.
[91] E.J. Prenner, R. Lewis, L.H. Kondejewski, R.S. Hodges, R.N. McElhaney, Differential scanning calorimetric study of the effect of the antimicrobial peptide gramicidin S on the thermotropic phase behavior of phosphatidylcholine, phosphatidylethanolamine and phosphatidylglycerol lipid bilayer membranes, Biochim. Biophys. Acta 1417 (1999) 211–223.
[92] W. Mobius, E. van Donselaar, Y. Ohno-Iwashita, Y. Shimada, H.F.G. Heijnen, J.W. Slot, H.J. Geuze, Recycling compartments and the internal vesicles of multivesicular bodies harbor most of the cholesterol found in the endocytic pathway, Traffic 4 (2003) 222–231.
[93] T. Shangguan, D. Alford, J. Bentz, Influenza-virus-liposome lipid mixing is leaky and largely insensitive to the material properties of the target membrane, Biochemistry 35 (1996) 4956–4965.
[94] A.A. Waheed, E.O. Freed, Lipids and membrane microdomains in HIV-1 replication, Virus Res. 143 (2009) 162–176.
[95] S.T. Yang, V. Kiessling, J.A. Simmons, J.M. White, L.K. Tamm, HIV gp41-mediated membrane fusion occurs at edges of cholesterol-rich lipid domains, Nature Chem. Biol. 11 (2015) 424–431.
[96] E. Sevcsik, G.J. Schutz, With or without rafts? Alternative views on cell membranes, Bioessays 38 (2016) 129–139.

Supplementary Information for Publication

^{2}H nuclear magnetic resonance spectroscopy supports larger amplitude fast motion and interference with lipid chain ordering for membrane that contains β sheet human immunodeficiency virus gp41 fusion peptide or helical hairpin influenza virus hemagglutinin fusion peptide at fusogenic pH

Ujjayini Ghosh and David P. Weliky*

Department of Chemistry, Michigan State University, East Lansing, MI, USA 48824

* email: weliky@chemistry.msu.edu; telephone: 517-353-1177; fax: 517-353-1153

Figure S1. ^{2}H NMR spectra of replicate GPfp (1:25) samples

Sample 1 spectra are displayed in Fig. 4 in the main text

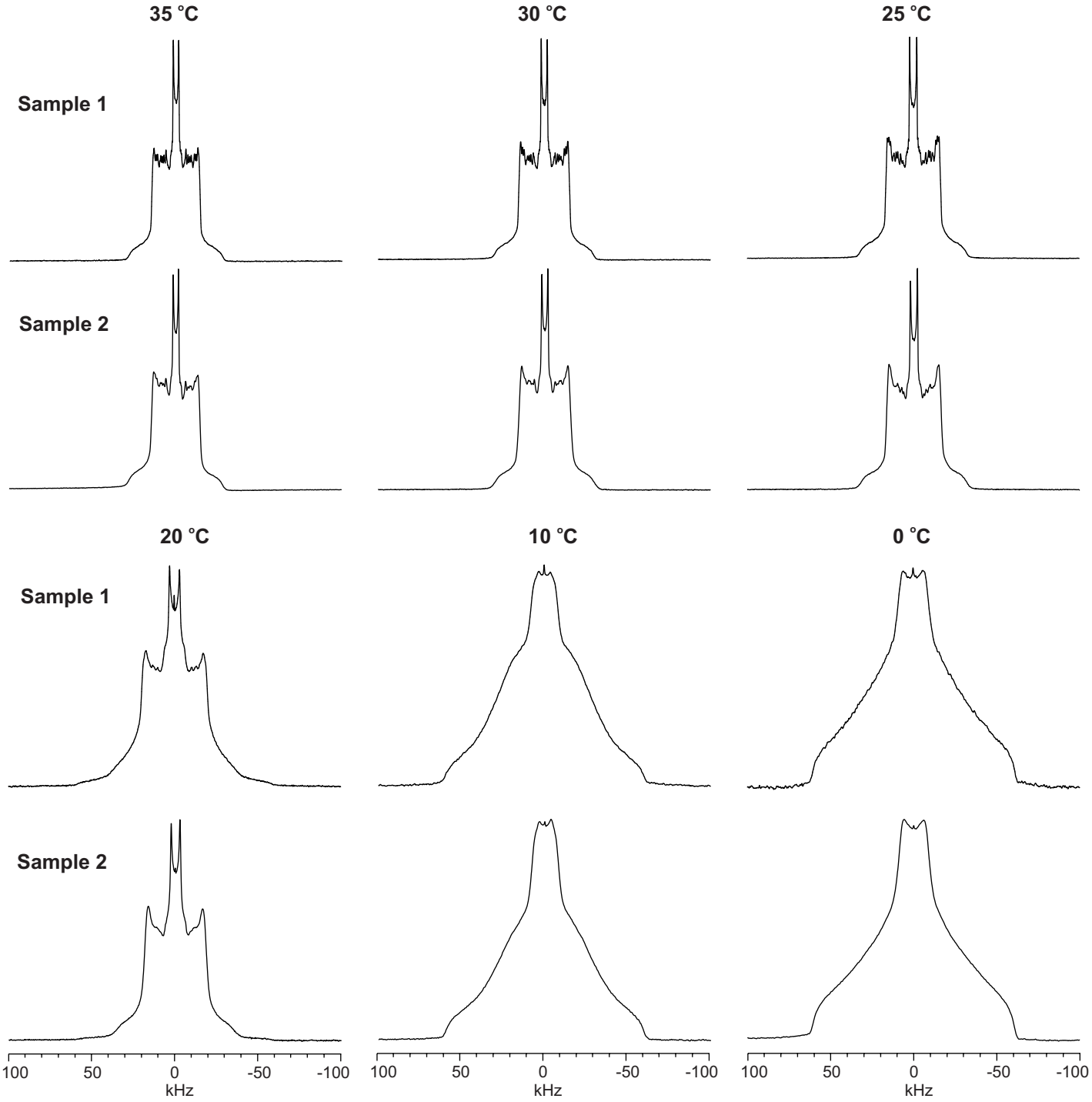

Figure S2. ^{2}H NMR spectra of replicate samples at 35 °C

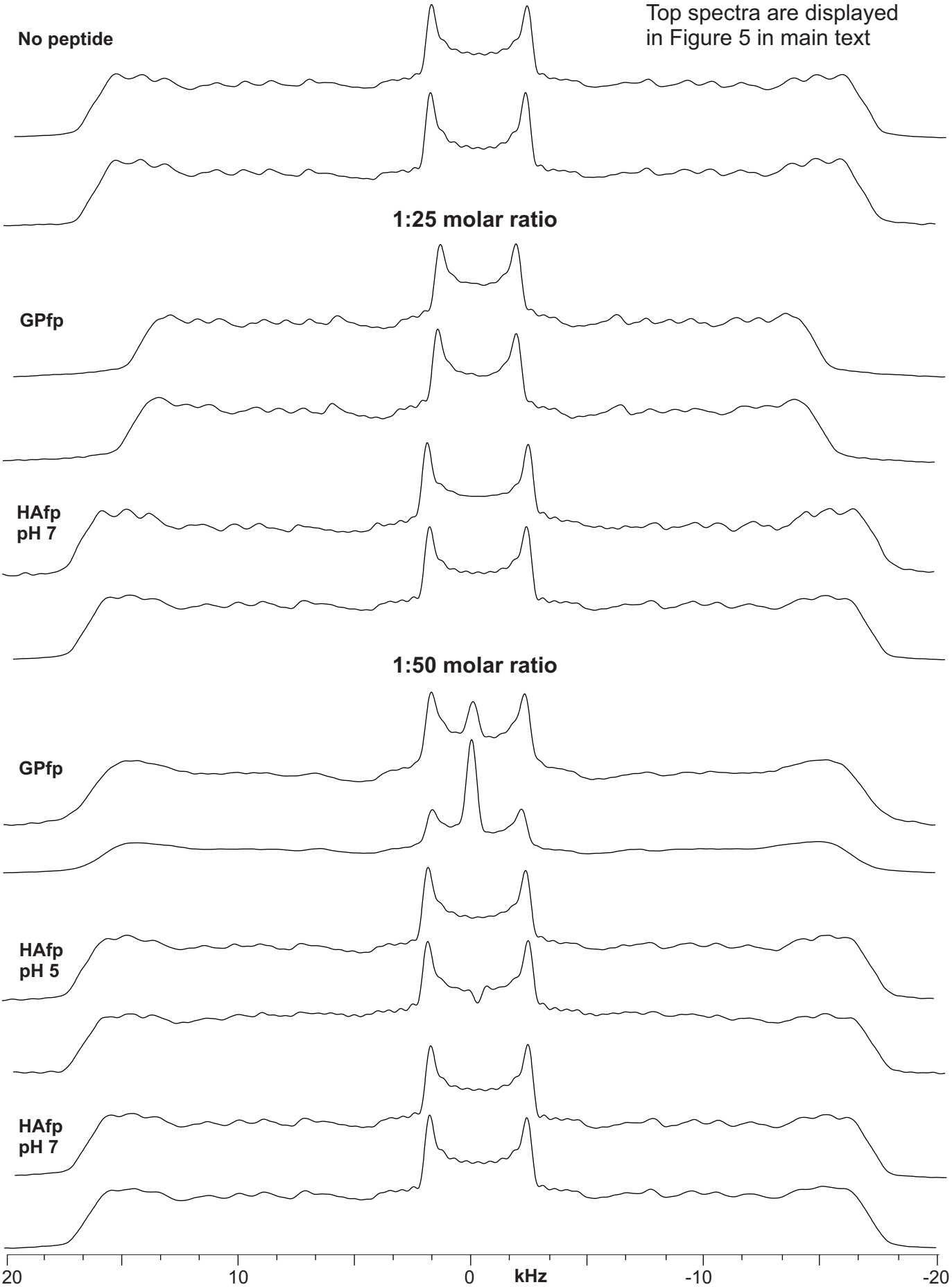

Table S1. Order parameters of DMPC-d54 at 35 ^{o}C [a]

Carbon number	no peptide		GPfp		HAfp pH 7	
	Sample					
	A	B	C	D	E	F
2-6	0.2538	0.2540	0.2225	0.2217	0.2610	0.2601
7	0.2335	0.2341	0.1957	0.2011	0.2435	0.2416
8	0.2181	0.2179	0.1792	0.1835	0.2268	0.2246
9	0.1920	0.1936	0.1583	0.1604	0.2010	0.1967
10	0.1829	0.1792	0.1490	0.1536	0.1888	0.1876
11	0.1627	0.1656	0.1328	0.1386	0.1701	0.1664
12	0.1449	0.1439	0.1166	0.1218	0.1502	0.1494
13	0.1187	0.1193	0.0980	0.1012	0.1252	0.1227
14	0.0350	0.0339	0.0285	0.0281	0.0360	0.0356

[a] Each S_{CD} order parameter is determined from a $\Delta\nu$ splitting of the de-Paked spectra with $S_{CD} = (\Delta\nu)/334$ kHz. Samples with peptide were prepared with 1:25 peptide:lipid molar ratio. Table 1 in the main text is based on spectra for samples A, C, and E.